DETONATION PROPAGATION THROUGH U-BENDS

S. M. Frolov, V. S. Aksenov, and I. O. Shamshin

N. N. Semenov Institute of Chemical Physics
Russian Academy of Sciences
Moscow, Russia

The objective of the research outlined in this paper is to provide experimental and computational data on initiation, propagation, and stability of gaseous fuel–air detonations in tubes with U-bends implying their use for design optimization of pulse detonation engines (PDEs). The first experimental results with the U-bend of a fixed curvature indicate that, on the one hand, the U-bend of the tube promotes the shock-induced detonation initiation. On the other hand, the detonation wave propagating through the U-bend is subjected to temporary attenuation followed by the complete recovery in the straight tube section downstream from the U-bend. Numerical simulation of the process reveals some salient features of transient phenomena in U-tubes.

Introduction

Tube bends and coils are the elements, which can be used for elongating the detonation tubes of PDEs to ensure reliable deflagration-to-detonation transition (DDT). Surprisingly little work has been done on the DDT and detonation diffraction in such elements [1, 2]. Authors' recent research on a liquid-fueled air-breathing PDE [3–5] has unequivocally demonstrated that tube coils do promote DDT efficiently. It is anticipated that depending on the tube diameter, U-bend curvature, and the characteristic lengths of tube segments attached to the U-bends, different diffractions of initiating shock waves and developed detonations can result in various transient phenomena leading to shock-to-detonation transition or failure of a developed detonation.

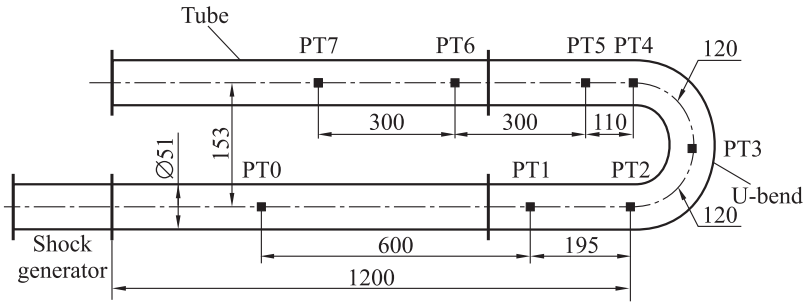

Figure 1 Schematic of the experimental setup for the studies of detonation initiation and propagation in tubes with U-bends. Dimensions are in mm

The objective of the research outlined in this paper is to provide experimental and computational data on gaseous fuel–air detonations propagating in tubes with U-bends and to derive theoretical criteria for evaluating detonation initiation and stability conditions in terms of tube diameter, U-bend curvature, and characteristic lengths of tube segments between the U-bends. The main configuration to be studied is shown in Fig. 1.

Experimental Setup

Figure 1 shows the schematic of the experimental setup for the studies of detonation initiation and propagation in tubes with U-bends. The setup comprises the Shock Generator, two pieces of straight tube 51 mm in inner diameter, and a U-bend made of the tube of the same diameter. The far end of the tube opposite to the Shock Generator is closed. The setup allows replacing the U-bends to study the effect of their curvature on detonation initiation and propagation. The internal radius of the U-bend shown in Fig. 1 is equal to tube diameter, i.e., 51 mm.

The Shock Generator is a combustion chamber 22 cm^3 in volume equipped with a changeable nozzle of up to 14 mm in diameter closed with a bursting diaphragm. Before the run, the combustion chamber is filled with a solid propellant (the mass up to 2.5 g). The propellant is ignited by an igniter 0.2 ± 0.02 g in mass. The maximal pressure in the

chamber is 100 MPa. The strength of the shock wave formed depends on the nozzle diameter, diaphragm thickness, and thermodynamic parameters of combustion products in the Shock Generator.

Before each run, the detonation tube is evacuated and filled with the stoichiometric propane–air mixture at initial pressure of 0.1 MPa and initial temperature of 294 ± 2 K.

The measuring system includes piezoelectric pressure transducers, analog-to-digital converter, and a PC. The pressure transducers PT0, PT1, ..., PT7 are mounted along the tube as shown in Fig. 1. The pressure transducer PT0 is used for triggering the measuring system.

The velocity of the shock wave was calculated using the formula $V = X/\Delta t$, where X is the length of the measuring segment and Δt is the time interval determined from the records of pressure transducers. The measuring segments PT0–PT1, PT1–PT2, ..., PT6–PT7 correspond to the segments between the pressure transducers PT0 and PT1, PT1 and PT2, ..., PT6 and PT7, respectively. The error in determining X is ± 0.5 mm which gives about 0.5% error for the shortest measuring segment (PT4–PT5) 110 mm long. The time interval Δt is determined at the half-amplitude levels of pressure-transducer signals. Because of the finite dimensions of the sensitive elements of the transducers, the duration of the shock (and detonation) front registration is not less than 3 μs. The characteristic sampling time of each measuring channel is 1.2 μs, which allows the resolution of the wave front with two to three samples. Thus, the time interval Δt was determined with an uncertainty of ± 2.4 μs. The detonation velocity in the stoichiometric propane–air mixture is at the level of 1800 m/s. The mean time interval taken for the detonation wave to pass the shortest measuring segment PT4–PT5 is about 61 μs. Hence, the maximal error in determining the time interval Δt is $\pm 4\%$, and the corresponding error of determining the shock and detonation wave velocity does not exceed 5%. The lengths of the measuring segments PT2–PT3 and PT3–PT4 in the U-bend are measured along the arc and are equal to 120 mm.

Experimental Results

Table 1 and Fig. 2 show the shock wave velocities measured at different measuring segments of the tube in 5 representative runs: Run 1 to

Table 1 Measured shock wave velocities (in m/s) at different measuring segments of the tube with the U-bend of Fig. 1

Measuring segment	Run 1	Run 2	Run 3	Run 4	Run 5
PT0–PT1	602 ± 6	862 ± 9	1007 ± 10	1117 ± 11	1750 ± 18
PT1–PT2	575 ± 12	805 ± 6	1083 ± 22	1242 ± 25	1741 ± 35
PT2–PT3	585 ± 20	800 ± 25	1052 ± 32	1071 ± 35	1739 ± 50
PT3–PT4	588 ± 20	759 ± 25	1071 ± 33	1263 ± 40	1690 ± 50
PT4–PT5	544 ± 17	769 ± 25	1038 ± 32	1310 ± 40	1507 ± 45
PT5–PT6	534 ± 15	696 ± 18	1215 ± 30	1754 ± 45	1744 ± 45
PT6–PT7	517 ± 13	—	2027 ± 50	1785 ± 45	—

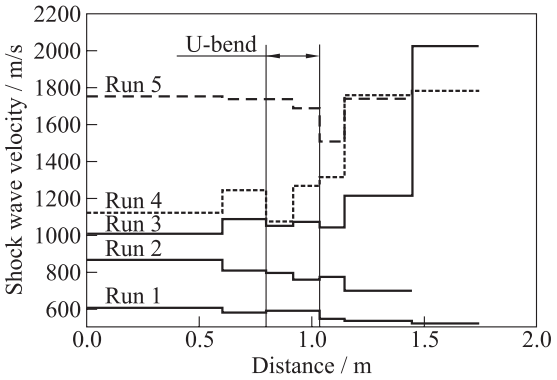

Figure 2 Mean shock wave velocities at different measuring segments of the tube with the U-bend in 5 representative runs

Run 5. Note that these runs are well reproducible at similar initial conditions. Figures 3*a* to 3*e* show the pressure records registered by pressure transducers PT1 to PT7 in these runs. Note that the pressure scales in Figs. 3*a* to 3*e* are approximate as different pressure transducers have slightly different sensitivities.

In Run 1, the mean shock wave velocity at the entrance to the U-bend (measuring segment PT1–PT2) is about 575 m/s. The velocity of the shock wave decreases gradually with the distance traveled, although in the U-bend, it is nearly constant (~ 580 m/s), see Fig. 2.

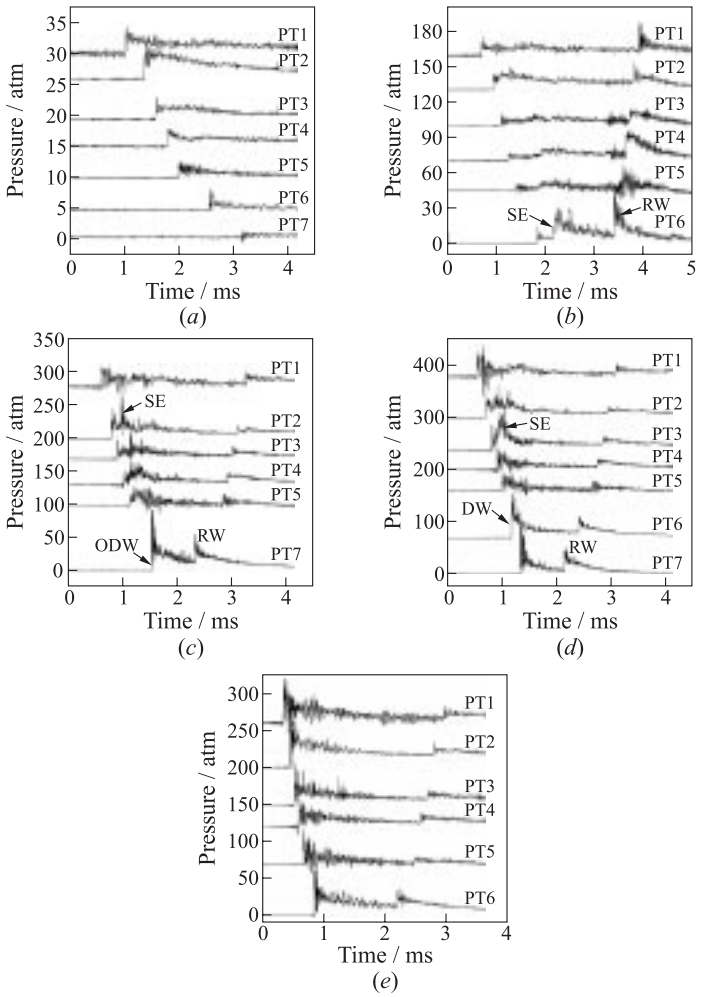

Figure 3 Pressure records registered by the pressure transducers PT1 to PT7 in 5 representative runs with different mean shock wave velocities at the entrance to the U-bend (measuring segment PT1–PT2): (*a*) Run 1, $V = 575$ m/s; (*b*) Run 2, $V = 805$ m/s; (*c*) Run 3, $V = 1083$ m/s; (*d*) Run 4, $V = 1242$ m/s; and (*e*) Run 5, $V = 1741$ m/s

In Run 2, the mean shock wave velocity at the entrance to the U-bend is somewhat higher (about 805 m/s) than in Run 1. Nevertheless, the qualitative behavior of the shock wave is similar to that in Run 1 (see Fig. 2) except for the indication of the secondary explosion (SE) on the record of PT6 at $t \approx 2200$ μs (see Fig. 3*b*). Also, at $t \approx 3400$ μs, one can see the reflected blast wave (RW) appearance on the record of PT6. This blast wave propagates upstream at a velocity of 1740 m/s at the measuring segment PT6–PT5, 1530 m/s at PT5–PT4, 1580 m/s at PT4–PT3, 1645 m/s at PT3–PT2, and 1670 m/s at PT2–PT1, i.e., the reflected blast wave resembles a detonation wave in terms of its propagation velocity. Note that in the straight tube of the same length, neither a secondary explosion nor a reflected, detonation-like wave were observed, other conditions being similar.

In Run 3, the mean shock wave velocity at the entrance to the U-bend is about 1083 m/s, i.e., higher than in Run 2. The shock wave traverses the U-bend at a nearly constant velocity of about 1060 m/s but suddenly accelerates to 1215 m/s at the measuring segment PT5–PT6 and to 2027 m/s at the measuring segment PT6–PT7 (see Fig. 2). The latter value of the shock wave velocity corresponds to the overdriven detonation wave (ODW). The reflected blast wave appearing at $t \approx 2300$ μs on the record of PT7 (see Fig. 3*c*) propagates upstream at the velocity of 1176 m/s at the measuring segment PT7–PT6, 1235 m/s at PT6–PT5, 1295 m/s at PT5–PT4, 1165 m/s at PT4–PT3, 1481 m/s at PT3–PT2, and 1234 m/s at PT2–PT1. This wave propagates in a partially reacted mixture as indicated by the records of pressure transducers PT2 to PT5 exhibiting secondary explosions and pressure humps. Therefore, its propagation velocity is lower than in Run 2.

In Run 4, the mean shock wave velocity at the entrance to the U-bend is about 1242 m/s, i.e., higher than in Run 3. When entering the U-bend, the shock wave first decelerates to 1071 m/s at the measuring segment PT2–PT3 and then accelerates to 1263 m/s at the measuring segment PT3–PT4. This acceleration is most probably caused by the secondary explosion clearly seen on the record of the pressure transducer PT3 in Fig. 3*d*. After passing the U-bend, the shock wave continues accelerating and transitions to a detonation wave (DW) propagating at a velocity of 1750–1800 m/s at the measuring segments PT5–PT6 and PT6–PT7 (see Fig. 2). The reflected blast wave appearing at $t \approx 2100$ μs on the record of PT7 (see Fig. 3*d*) propagates upstream at the

velocity of 1167 m/s at the measuring segment PT7–PT6, 1162 m/s at PT6–PT5, 1294 m/s at PT5–PT4, 1212 m/s at PT4–PT3, 1364 m/s at PT3–PT2, and 1274 m/s at PT2–PT1. This wave propagates at nearly the same velocity as in Run 3.

In Run 5, the mean shock wave velocity at the entrance to the U-bend, i.e., at the measuring segment PT1–PT2, is about 1741 m/s. At the measuring segment PT0–PT1, its velocity is about 1750 m/s. This propagation velocity is close to the Chapman–Jouguet (CJ) detonation velocity for the stoichiometric propane–air mixture at normal conditions. When traversing the U-bend, the detonation wave decelerates to 1690 m/s at the measuring segment PT3–PT4 and then to 1507 m/s at the measuring segment PT4–PT5 after exiting the U-bend. However, it accelerates again to the initial propagation velocity of 1744 m/s at the measuring segment PT5–PT6 (see Fig. 2). The reflected blast wave appearing at $t \approx 2160$ μs on the record of PT6 (see Fig. 3*e*) propagates upstream at the velocity of 1063 m/s at the measuring segment PT6–PT5, 1089 m/s at PT5–PT4, 1121 m/s at PT4–PT3, 1154 m/s at PT3–PT2, and 1174 m/s at PT2–PT1. This velocity is somewhat higher than the sound speed in the detonation products of the stoichiometric propane–air mixture ($\sim$ 990 m/s).

Computational Approach

The mathematical model is based on the standard two-dimensional (2D) Euler equations, energy conservation equation with a chemical source term, and equation of chemical kinetics. The kinetics of propane oxidation was modeled by a single-stage overall reaction

$$C_3H_8 + 5O_2 \rightarrow 3CO_2 + 4H_2O \qquad (1)$$

The combustion heat of propane is taken equal to 46.6 MJ/kg. The expression for the bimolecular reaction rate $w = k[C_3H_8][O_2]$ was used to calculate the rate of reaction (1), where k is the rate constant ($k = 2.1 \cdot 10^{15} P^{-0.2264} \exp(-E/(RT))$ cm^3/(mol·s), T is the temperature, R is the gas constant, $E = 45460$ cal/mol is the activation energy, and P is pressure in atm). The rate constant was obtained by fitting the calculated ignition delays with the experimental data [6, 7] on ignition of the stoichiometric propane–air mixture behind reflected

Table 2 Ignition delays of the stoichiometric propane–air mixture

P, MPa	0.1					3.0	
T_0, K	1200	1400	1600	1800	2000	1200	1600
τ_{calc}, μs	2250 (1250)	250 (195)	49 (30)	13 (9)	5 (4)	161 (97)	4 (2)
$\tau_{\text{exp}1}$, μs	3700	330	55	13	5	407	6
$\tau_{\text{exp}2}$, μs	1500	130	10	—	—	140	1

shock waves. In the calculations, a zero-dimensional, constant-volume reaction kinetics was considered. Two definitions of the ignition delay were used: (*i*) as time corresponding to the maximal temperature rise (crossing of the tangent to this point at the time-history curve with the time axis) and (*ii*) as time corresponding to the characteristic ignition temperature $T = T_0 + RT_0^2/E$, where T_0 is the initial temperature. Table 2 shows the comparison between predicted τ_{calc} and measured $\tau_{\text{exp 1}}$ [6] and $\tau_{\text{exp 2}}$ [7] data. The 'experimental' results for a pressure of 3.0 MPa are the extrapolations of low-pressure measurements in [6, 7]. Two predicted values of τ_{calc} are presented: one corresponding to definition (*i*), and the other corresponding to definition (*ii*) (shown in brackets). A reasonable agreement between predicted and measured data is seen from the table.

For numerical solution of governing equations, a method of splitting by physical processes [8] was used. At each time step, at the first stage, only convective fluxes and pressure work were taken into account. This stage of integration was solved by the second-order Godunov–Kolgan method [9]. Mass, momentum, and energy fluxes through faces of a computational mesh were found from the exact solutions of the Riemann problem. At the second stage, the chemical reaction was taken into account. The fourth order Runge–Kutta method was used to integrate the reaction kinetic equation. A more detailed description of the numerical procedure is available in [10].

Results of Calculations

In the calculations, the same (but planar 2D) U-tube configuration as shown in Fig. 1 was studied. The tube was initially filled with the stoichiometric propane–air mixture at $P = 0.1$ MPa and $T_0 = 298$ K. A pla-

nar detonation wave was initiated by a short (10 mm long) tube section filled initially with the high-temperature (2500 K) and high-pressure (20 MPa) air simulating a Shock Generator of Fig. 1. The computational grid was uniform and contained 1600×400 square meshes with a size of 0.5 mm. The pressure histories at multiple locations along the symmetry surface of the U-tube, as well as along its internal and external walls were stored during the calculations. Based on these numerical 'pressure records,' the corresponding propagation velocities of the lead shock front were calculated. In addition, 2D flow fields were stored to visualize the flow pattern.

Figure 4 shows the predicted shock velocities along the internal wall (a), symmetry surface (b), and external wall (c) of the U-tube. The shock velocity is normalized by the CJ detonation velocity D_0. It is seen that the initial planar detonation wave (at $L < 0$) is slightly overdriven when it enters the U-bend (the region between the vertical dashed lines). Inside the U-bend, the lead shock front of the planar detonation wave starts to interact with compressive and expensive surfaces of the U-bend. As a result, different portions of the lead front exhibit different behavior due to temporally and spatially shifted interaction with compression and rarefaction waves and due to finite rate of chemical reaction. At the internal wall (Fig. 4a), the shock velocity decreases to nearly $0.4D_0$ in the middle of the U-bend, which is caused by the rarefaction fan at the expensive surface. Subsequent velocity spike (of about $1.2D_0$) is caused by a secondary explosion discussed below. Nevertheless, after this localized explosion, the shock velocity at the internal wall of the U-bend decreases again to nearly $0.4D_0$. Once the lead shock wave exits from the U-bend section, a second spike in its propagation velocity reaching $1.5D_0$ is observed which evolves similar to the first spike. During the subsequent evolution, the lead shock velocity oscillates around the D_0 value. The oscillations are driven by shock interactions with transverse waves.

At the symmetry surface (Fig. 4b), the evolution of the lead shock is somewhat different. On the entry to the U-bend, it exhibits a slight velocity increase followed by a decrease to about $0.65D_0$. Subsequent complex wave interactions result in several velocity spikes (up to $1.2D_0$) in the U-bend. The highest velocity spike (up to $1.4D_0$) is attained at the exit from the U-bend. Similar to Fig. 4a, further evolution of

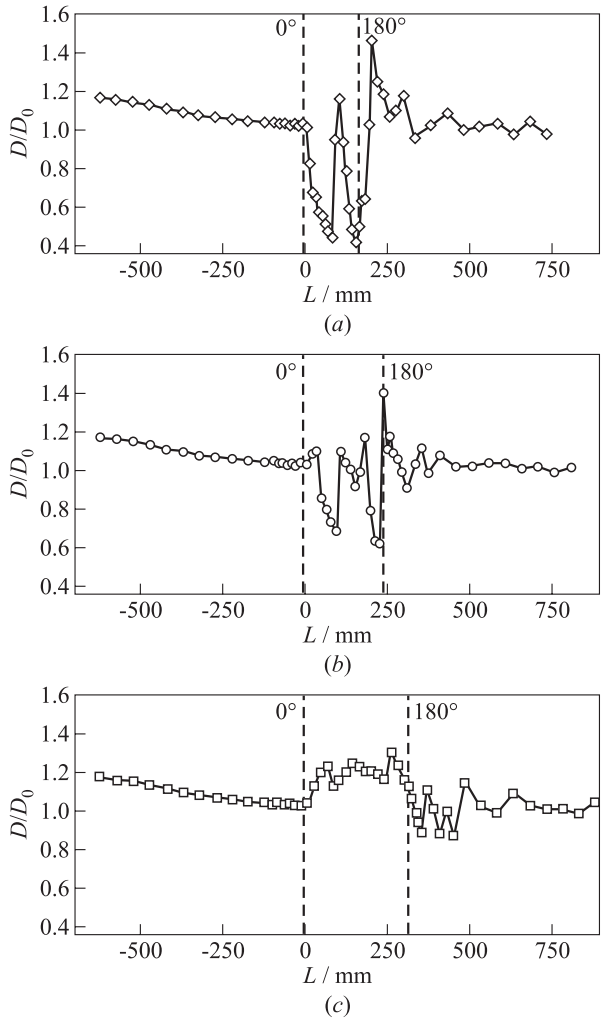

Figure 4 Predicted normalized shock velocities along the internal wall (*a*), symmetry surface (*b*), and external wall (*c*) of the U-tube. The origin of the X-axis is located at the tube cross-section corresponding to the entrance to the U-bend. The region between the vertical dashed lines corresponds to the U-bend section

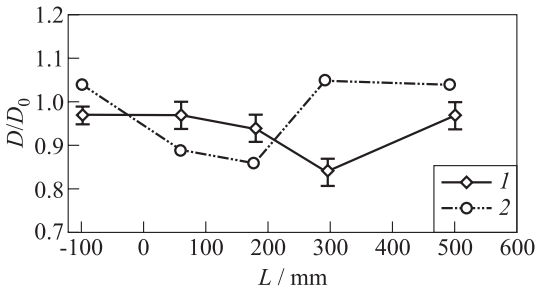

Figure 5 Comparison of normalized predicted and measured shock velocities along the symmetry surface of the U-tube. The origin of the X-axis is located at the tube cross-section corresponding to the entrance to the U-bend: *1* — experiment and *2* — calculation

the lead shock velocity at the symmetry surface exhibits attenuating oscillatory behavior with the average value of D_0.

At the external wall (Fig. 4*c*), the propagation velocity of the lead shock wave in the U-bend corresponds to the overdriven detonation with the overdrive ratio of 1.2–1.3. Once the wave exits from the U-bend, its propagation velocity decreases below $0.9D_0$ and attains the average D_0 value in an oscillatory manner.

Figure 5 compares normalized predicted and measured shock velocities along the symmetry surface of the U-tube. A good qualitative agreement of the results is worth noting. The quantitative differences in the values of wave velocities could be attributed to three-dimensional (3D) effects pertinent to experiments and simplified assumptions adopted in the model.

Figure 6 shows predicted normalized shock velocities in the U-bend as a function of the polar angle α and the calculated pressure histories at different locations along the U-bend. The pressure histories relevant to $\alpha = 0°$ (low left corner) indicate that the initially planar detonation front exhibits pressure disturbances in the wake. The first evidence of the compression wave appears on the pressure curve at the external wall. This compression propagates towards the internal wall. At $\alpha = 45°$, a considerable pressure drop at the internal wall and symmetry surface is observed, whereas the pressure trace at the external wall shows the

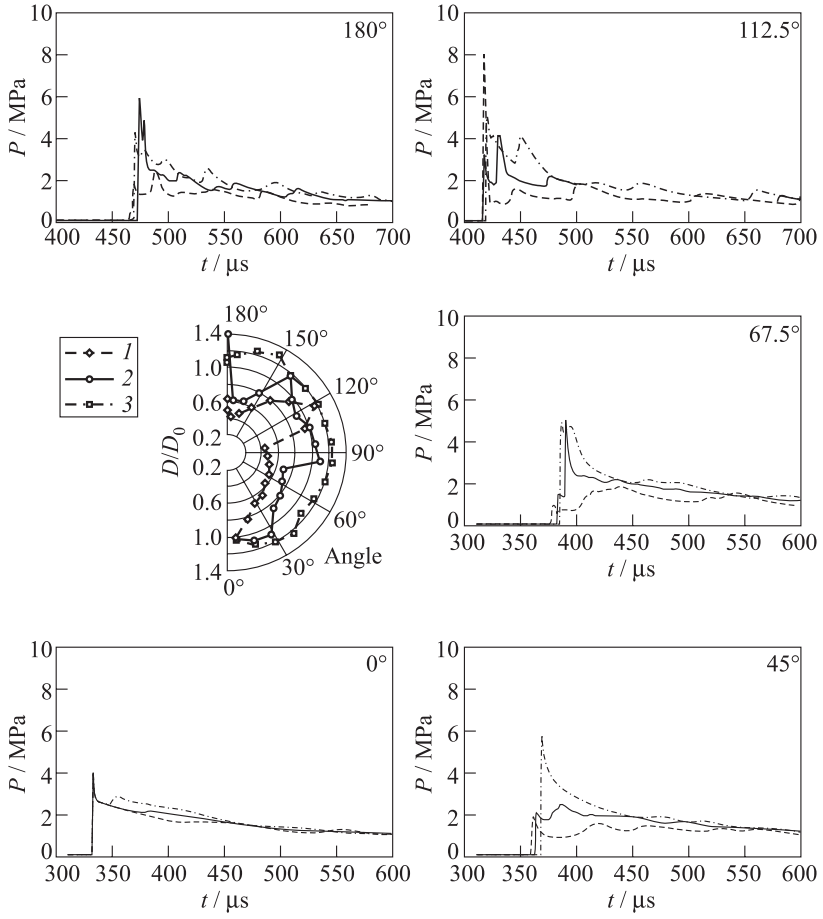

Figure 6 Predicted normalized shock velocities in the U-bend as a function of the polar angle and the calculated pressure histories at different locations along the internal wall (*1* and dashed curves), symmetry surface (*2* and solid curves), and external wall (*3* and dash-and-dot curves) of the U-tube and different polar angles (shown in the upper right corners)

existence of the overdriven detonation. At $\alpha = 67.5°$, the shock pressure at the internal wall attains a nearly minimal value, which is consistent with the minimal shock velocity in Fig. 4*a* or at the velocity diagram of Fig. 6. Note that the pressure curve at the internal wall has a pressure hump characteristic of a secondary explosion (see, e.g., Fig. 3*d*). This secondary explosion results in an extremely high-pressure spike (above 8 MPa) at the internal wall at $\alpha = 112.5°$. At the exit from the U-bend, the wave structure differs considerably from the planar incident wave at the U-bend entrance. Different portions of the lead front have different velocities and pressure amplitudes. The tails of the pressure traces exhibit regular oscillations.

Figures 7 to 9 show the predicted evolution of pressure (Fig. 7) and propane mass fraction (Fig. 8) fields as well as maximal pressure footprint (Fig. 9) at propagation of a detonation wave in the U-tube. The mechanism of the secondary explosions at the internal wall is clearly indicated by Figs. 7 and 8. Joint consideration of Figs. 7*b* and 8*b* reveals that there is an unburned fuel behind a weak shock wave in the vicinity to the internal wall. A strong transverse shock wave is evident in Fig. 7*b* which leads to fast localized fuel consumption behind its front. Also, one can see the pockets of unburned fuel far behind the lead shock formed in the tail of this transverse wave and in the region near the internal wall. Figure 7*f* shows the other secondary explosion in the vicinity of the internal wall appearing as a high-pressure zone. The mechanism of its origin is the same as discussed above. Similar to Fig. 8*b*, unburned fuel pockets far behind the lead shock front can be seen in Fig. 8*f*.

Figure 9 shows the establishment of the cellular structure in the wave passing through the U-band. It takes about 8–10 tube diameters for the detonation wave to attain a regular cellular structure after exiting from the U-band. Density disturbances in the wake of the propagating detonation also disappear at 8–10 tube diameters.

Concluding Remarks

Thus, the experimental results obtained in a tube with a U-bend demonstrate a considerable effect of the U-bend on detonation initiation and propagation. On the one hand, the U-bend of the tube promotes the shock-induced detonation initiation as shown in experimental Runs 2

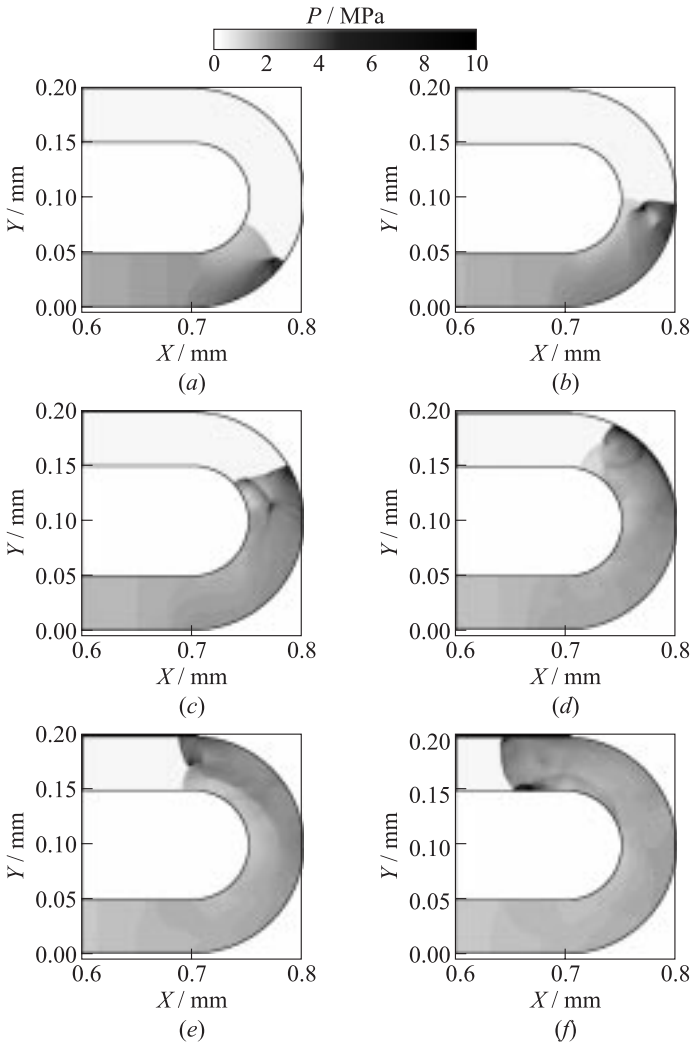

Figure 7 Predicted evolution of the pressure field at propagation of a detonation wave through the U-bend. The snapshots (*a*) to (*f*) are plotted with a time interval of 25 μs

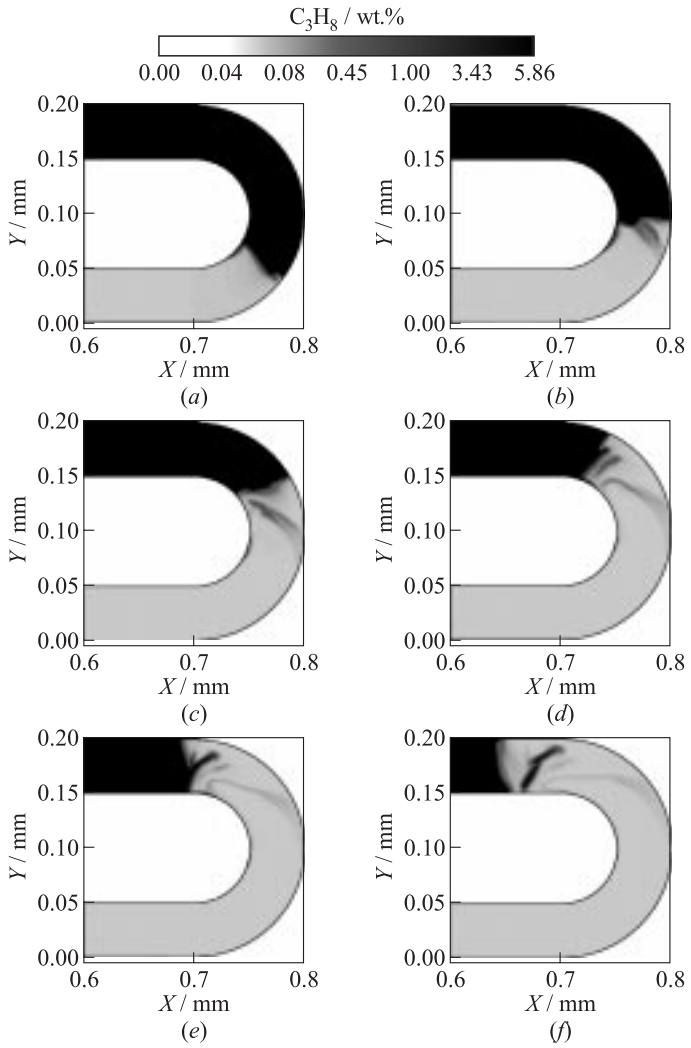

Figure 8 Predicted evolution of the propane mass fraction field at propagation of a detonation wave through the U-bend. The snapshots (*a*) to (*f*) are plotted with a time interval of 25 μs

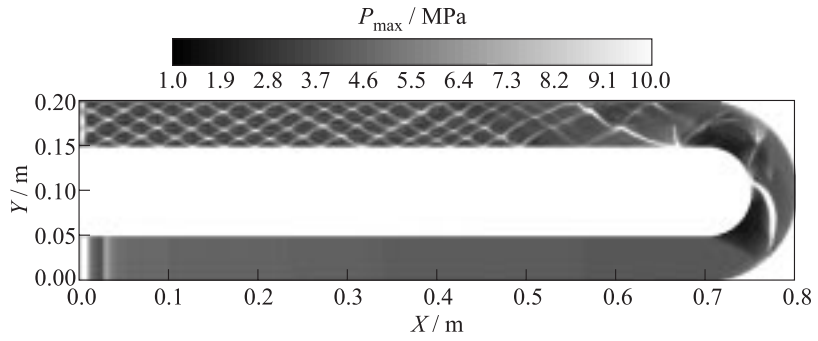

Figure 9 Maximal pressure footprint at propagation of a detonation wave in the U-tube indicating the formation of a cellular detonation structure

to 4. On the other hand, the detonation wave propagating through the U-bend is subjected to temporary attenuation with the velocity drop of about 250 m/s (15%) followed by the recovery of the propagation velocity in the straight tube section downstream from the U-bend, as shown in experimental Run 5.

Two-dimensional numerical simulation of detonation transition through the U-bend reveals salient features of transient phenomena in U-tubes. It is shown that different portions of the lead detonation front exhibit different behavior in the U-bend due to temporally and spatially shifted interaction with compression and rarefaction waves and due to finite rate of chemical reaction. Both localized detonation decay and detonation reinitiation events were detected near the internal wall of the U-bend. In addition, large-scale unburned fuel pockets far behind the lead shock front were shown to form during detonation transition through the U-bend. After exiting from the U-bend, the detonation recovers at a distance of about 8–10 tube diameters attaining an established cellular structure.

The curvature of the U-bend and tube diameter are expected to be the most important governing parameter of the problem which determine the evolution of the initiating shock wave or a developed detonation wave in such a system. The future work will be concentrated on further experimental and computational studies of the encountered phenomena.

Acknowledgments

This work was partly supported by the U.S. Office of Naval Research and International Science and Technology Center. Dr. I. Shamshin also acknowledges the support of REC 011 "Fundamental investigation of matter under extreme conditions" and CRDF within the program "Basic Research and Higher Education."

References

1. Nettleton, M. A. 1987. *Gaseous detonations: Their nature, effects and control.* London–New York: Chapman and Hall.
2. Frolov, S. M., V. S. Aksenov, and V. Ya. Basevich. 2005. Decreasing the predetonation distance in a drop explosive mixture by combined means. *Doklady Physical Chemistry* 401(1):28–31.
3. Frolov, S. M., V. Ya. Basevich, and V. S. Aksenov. 2004. Liquid-fueled PDE with externally driven shock-to-detonation transition. In: *17th ONR Propulsion Meeting Proceedings.* Eds. G. Roy, and A. Ghoniem. Cambridge, MA: MIT Publ. 181–86.
4. Frolov, S. M., V. S. Aksenov, and V. Ya. Basevich. 2005. Air-breathing liquid-fueled pulse detonation engine demonstrator. *Doklady Physical Chemistry* 402(2):93–95.
5. Frolov, S. M. 2006 (in press). Liquid-fueled air-breathing PDE demonstrator. *J. Propulsion Power* 22.
6. Burcat. A., K. Scheller, and A. Lifshitz. 1971. Shock tube investigation of comparative ignition delay times for C1–C5 alkanes. *Combustion Flame* 16(3):29.
7. Borisov, A. A., V. M. Zamanskii, V. V. Lissianskii, G. I. Skatchkov, K. Ya. Troshin, and I. M. Baranov. 1988. Kinetics of energy release at high-temperature ignition of hydrocarbons in air and oxygen. *Chemical Physics Reports* 7(5):665.
8. Kovenya, V. M., and N. N. Yanenko. 1981. *Splitting method in gasdynamic problems.* Novosibirsk: Nauka.
9. Kolgan, V. P. 1972. Application of principle of minimal derivative to construction of a finite-difference scheme for calculation of gasdynamic discontinuities. *Uchenye Zapiski TsAGI* 3:68.
10. Borisov, A. A., S. I. Sumskoi, I. O. Shamshin, P. V. Komissarov, M. A. Silakova, A. E. Mailkov, and R. N. Elshin. 2002. Numerical and experimental modeling of explosive transformation of aluminum and ammonium nitrate at their injection to the tube followed by their dicharge to the open space. *Chemical Physics Reports* 21(5):97.